Journal of Sound and Vibration (2002) **256**(2), 347–365
doi:10.1006/jsvi.2001.4212, available online at http://www.idealibrary.com on IDEAL®

LIMIT-CYCLE STABILITY REVERSAL NEAR A HOPF BIFURCATION WITH AEROELASTIC APPLICATIONS

D. Dessi

INSEAN, via di Vallerano 139, 00128 *Rome, Italy. E-mail: d.dessi@insean.it*

F. Mastroddi

Aerospace Department, University of Rome "La Sapienza", via Eudossiana, 16, *I*-00184 *Rome, Italy. E-mail: franco@mastroddi.ing.uniroma1.it*

AND

L. Morino

Department of Mechanical and Industrial Engineering, University of Rome "Roma Tre", Via della Vasca Navale, 79, *Rome, Italy. E-mail: L.Morino@uniroma3.it*

(*Received* 15 *May* 2001, *and in final form* 20 *November* 2001)

The objective of this paper is to present an analytical/numerical analysis of the phenomenon of limit-cycle stability reversal (from unstable to stable, and *vice versa*). A singular perturbation technique, the method of the normal form (in the asymptotic-expansion version), is utilized. The number of equations is then reduced to a "minimal set", for which the results are in good agreement with those from the original equations. This minimal set is determined by the amplitude of the $\hat{\lambda}$-points (a concept closely related to the small divisors in the KAM theory). This set is larger than that corresponding to the zero real-part eigenvalues (center-manifold theorem). The method is applied to a specific problem: an aeroelastic section with cubic free-play non-linearities where the parameter μ is the flight speed. Numerical studies have been performed to show the dependence of the Hopf bifurcation characteristics upon the structural and geometric properties of the wing section. Plots depicting amplitudes and frequency versus flight speed are presented.

1. INTRODUCTION

A Hopf bifurcation denotes the phenomenon that occurs when *a* fixed-point solution becomes linearly unstable beyond a critical value (μ_c) of a parameter μ; in the non-linear case, a (stable or unstable) limit cycle solution appears in the neighborhood of μ_c. Such a bifurcation is denoted super-critical if there exists a stable limit cycle for $\mu > \mu_c$, or sub-critical if there exists an unstable limit cycle for $\mu < \mu_c$. Limit-cycle stability reversal here denotes the behavior of a system in which for a certain critical value of the parameter a low-amplitude unstable limit cycle and a high-amplitude stable limit cycle merge (and vice versa): such a critical point is known as the turning point.

This paper presents a general methodology for the analysis of a limit-cycle stability in the neighborhood of a Hopf bifurcation. The motivation for the paper stems from the interest of the authors in aeroelasticity. Thus the applications are limited to this field. However, the formulation is general and applicable to other fields as well.

0022-460X/02/$35.00

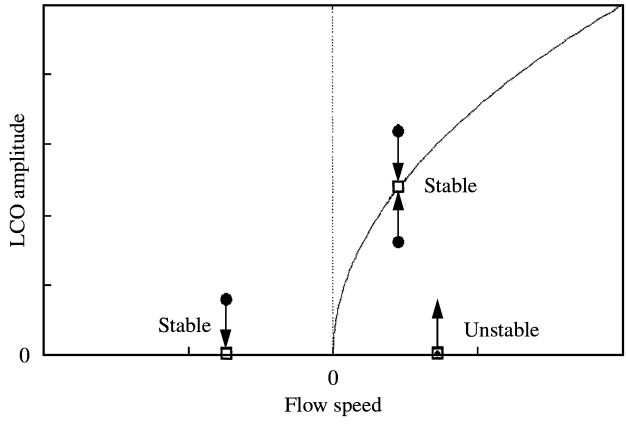

Figure 1. Super-critical Hopf bifurcation, pitchfork-like shape: □, equilibrium solution; ●, initial condition.

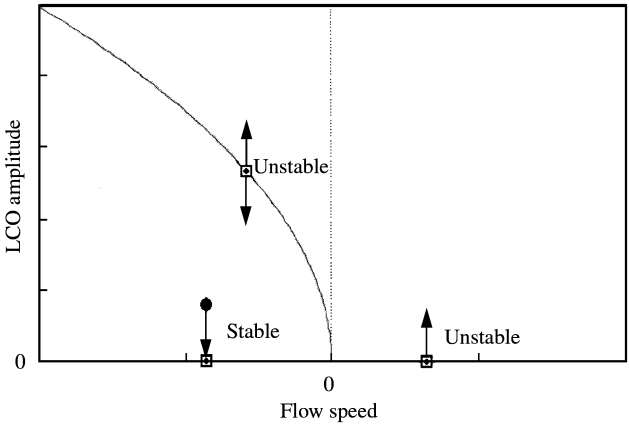

Figure 2. Sub-critical Hopf bifurcation, pitchfork-like shape. □, equilibrium solution; ●, initial condition.

Aeroelasticity deals with fluid–structure interactions. Here, one examines, in particular, the instability due to the interaction between an airplane wing and the flow surrounding it. If the instability involves oscillations, the phenomenon is called flutter, otherwise it is called divergence. This paper concentrates on flutter.

According to the linear flutter analysis, beyond a certain speed (here denoted as the flutter speed, U_F) the oscillations are not damped and their amplitude grows exponentially. The post-flutter behavior may be classified into two types: benign and explosive (or destructive) flutter. Specifically, in the first case, above the flutter speed, the system tends to stable limit cycle oscillations (LCOs) with an amplitude that grows in proportion to $\sqrt{U - U_F}$ provided that the values of $U - U_F$ are small. In the second case (again for small values of $U_F - U$), even below the linear flutter speed, the system may experience instability, provided that the initial conditions are sufficiently high: the initial-condition amplitude necessary to excite this instability varies in proportion to $\sqrt{U_F - U}$. In dynamical system terminology (see, e.g. reference [1]) these two phenomena are known, respectively, as stable and unstable limit cycles (see Figures 1 and 2). The first case — stable

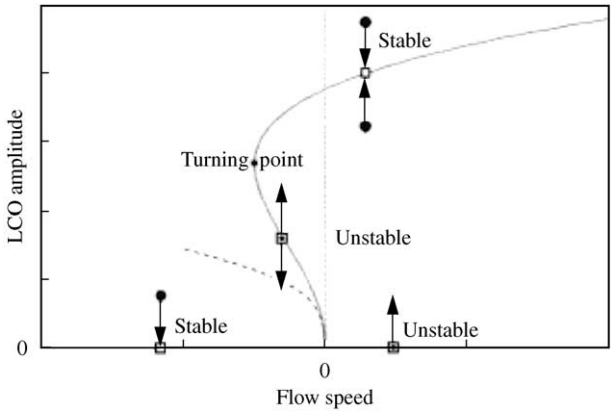

Figure 3. Sub-critical Hopf bifurcation with turning point. □, equilibrium solution; ●, initial condition.

limit cycle — is mathematically known as super-critical Hopf bifurcation; the second one as sub-critical Hopf bifurcation.

From a practical point of view, the second case (i.e. "explosive" or "destructive" flutter), implies that beyond the flutter speed U_F the system may experience a sudden onset of a destructive instability. This is a major design problem *per se.* However, an even more frightening implication is that the flutter speed is not at all a safe prediction, since this destructive instability may occur even below the flutter speed U_F, provided that the wing experiences initial conditions that are sufficiently high (such as those induced by a gust). It should be emphasized that such a non-linear analysis is never used in aircraft design.

Of course, as mentioned above, these considerations describe only the results of the small-amplitude non-linear analysis (specifically, third order, see below). However, there is experimental (see references [2–6]) as well as numerical [7–11] evidence that a combination of (1) a small-amplitude unstable limit cycle, and (2) a large-amplitudes stable limit cycle may occur for a given value of the flight speed, U. These merge at a critical speed. The point of the amplitude versus speed plane where this occurs is known as the *turning point*. In other words, there exists a possibility, under suitable initial conditions, of large-amplitude limit-cycle oscillations even below the flutter speed. Thus, it is desirable to have a more refined tool (fifth order analysis, see later) to investigate this behavior.

Such a high order analysis is the subject of this paper. The results indicate that the phenomenon discussed above is described by the amplitude versus velocity bifurcation plot depicted in Figure 3. This figure shows a sub-critical Hopf bifurcation which exhibits a turning point at a velocity lower than the flutter speed, determining a "knee" in the bifurcation diagram where the unstable limit-cycle (sub-critical Hopf bifurcation) reverses into a stable one (of course, a reversal from stable into unstable limit cycle is also possible, Figure 4). From an aeroelastic view point, this implies the possibility of a stable limit-cycle behavior below the flutter speed, U_F, provided that the initial condition is sufficiently large. For such a phenomenon an estimate of the turning-point speed may be achieved by analyzing the bifurcation diagram of Figure 3 described above. It may be noted that the third order analysis would predict the behavior prescribed by the dashed lines in Figures 3 and 4, which consists of horizontal parabolas (see references [12, 13]). Another question which needs to be answered is how to treat the variables corresponding to the eigenvalues which have negative real part.

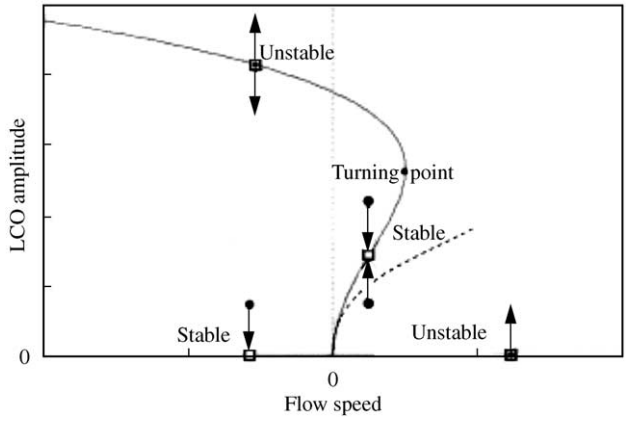

Figure 4. Super-critical Hopf bifurcation with turning point. □, equilibrium solution; ●, initial condition.

For small amplitudes, the state variables to be included in the analysis are determined by the center-manifold theorem (see, e.g. reference [1]). However, this is valid only in a small neighborhood of the Hopf bifurcation (e.g. a third order analysis†). Thus, the theorem is not applicable in the case of interest here because the amplitudes are not necessarily small (fifth order analysis). As a consequence of the above considerations, a criterion is introduced which allows one to identify the *minimal set* of state-space variables to be included in the analysis (minimal-set criterion; this is closely related to the concept of small divisors used in Hamiltonian mechanics). This criterion — arguably, the most significant contribution of the paper — is combined with a singular perturbation technique (the normal form method) to identify which terms in the equations of motion determine the system's non-linear behavior. This yields a convenient procedure to obtain an asymptotic expansion for the solution.

As a final observation, note that the stability characteristics of aeroelastic systems in the neighborhood of the flutter speed may be determined by both numerical-simulation or by singular-perturbation techniques. Numerical simulations do not give direct information (e.g. an analytic relationship) about the dependence of the stability properties upon, say, the wing characteristics; on the contrary, this may be obtained (although approximately) by singular perturbation techniques, which therefore may suggest how to modify some parameters in order to improve the flutter characteristics of the wing. On the other hand, numerical simulations have the advantage that they may yield results as accurate as desired (on the contrary, for analytical methods, the desired approximation is not necessarily achieved simply by increasing the number of terms retained in the asymptotic expansions, which are the basis of perturbation techniques; for asymptotic expansions do not guarantee convergence with the increase of the order, but only with the decrease of the expansion parameter, see reference [14]). Here both are used so as to exploit the advantages of both. Specifically, a methodology for analyzing fifth order non-linearities is presented. We then validate the results obtained with the fifth order analysis by comparing them with those obtained by numerical simulation, i.e. by direct numerical integration of the equations of motion.

The paper is based on the doctoral dissertation of Dessi [15]. The test case used is only that considered by Alighanbary and Price [10] (i.e. an airfoil elastically constrained by a linear translational spring and a non-linear torsional spring immersed in an

†The general formulation of the normal form method is well explained in references [1, 24–26].

incompressible inviscid flow); however, as mentioned above, the methodology has general validity.

2. BASIC NORMAL-FORM ANALYSIS

The objective of this section is to present the essentials of a general singular perturbation technique (the normal form method), which is based on the idea that a non-linear system can be simplified by a transformation in the phase space. This goal is achieved by two different steps: by reducing the number of equations (through the minimal-set criterion mentioned above) and by using the normal form method to eliminate in the reduced equations the non-linear terms that do not contribute significantly to the solution. For both steps, the selection is performed by introducing the 'near-resonance condition'. The methodology is presented, for the limited case of algebraic non-linearities (see footnote† of section 1).

Consider a one-parameter system of $N-1$ non-linear differential equations $\dot{z}_n = \mathscr{H}_n(z_n, \mu)$, with $N-1$ unknowns, and assuming that $\mathscr{H}_n(z_1, \ldots, z_{N-1}, \mu)$ be an analytic function (in particular a polynomial) of the variables $z_1, \ldots, z_{N-1}$ and the parameter μ, such that for $\mu > 0$ ($\mu < 0$) the system is linearly unstable (stable). It is convenient to treat μ as a dependent variable, $\mu = z_N$, which is governed by the equation $\dot{z}_N = 0$. Thus, the system may be written (assuming, with a minor loss of generality, that the linear terms may be recast in diagonal form) as

$$\dot{z}_n = \lambda_n z_n + \sum_{p,q=1}^{N} b_{npq} z_p z_q + \sum_{p,q,r=1}^{N} c_{npqr} z_p z_q z_r + \cdots \tag{1}$$

Then, setting $\mathbf{z} = \varepsilon \mathbf{x}$ yields‡

$$\dot{\mathbf{x}} = \mathscr{F}(\mathbf{x}, \varepsilon) = \mathbf{\Lambda}\mathbf{x} + \mathbf{f}(\mathbf{x}, \varepsilon) = \mathbf{\Lambda}\mathbf{x} + \varepsilon \mathbf{f}^{(1)}(\mathbf{x}, \mathbf{x}) + \varepsilon^2 \mathbf{f}^{(2)}(\mathbf{x}, \mathbf{x}, \mathbf{x}) + \cdots, \tag{2}$$

where $\mathbf{\Lambda}$ is a diagonal matrix, with $\mathbf{f}^{(1)}(\mathbf{x}_1, \mathbf{x}_2)$ is a symmetric bilinear form, $\mathbf{f}^{(2)}(\mathbf{x}_1, \mathbf{x}_2, \mathbf{x}_3)$ a symmetric trilinear form, and so on.

Next, consider the normal form method. The solution is given in terms of an asymptotic expansion of the type (near-identity transformation between $\mathbf{x}$ and $\mathbf{y}$)

$$\mathbf{x} = \mathscr{U}(\mathbf{y}, \varepsilon) = \mathbf{y} + \mathbf{u}(\mathbf{y}, \varepsilon) = \mathbf{y} + \varepsilon \mathbf{u}^{(1)}(\mathbf{y}) + \varepsilon^2 \mathbf{u}^{(2)}(\mathbf{y}) + \cdots + O(\varepsilon^{M+1}), \tag{3}$$

where the $\mathbf{u}^{(m)}$ are unknown functions of $\mathbf{y}$ which identify the transformation. One wishes to use equation (3) to transform equation (2) into an equation of the type

$$\dot{\mathbf{y}} = \mathscr{G}(\mathbf{y}, \varepsilon) = \mathbf{\Lambda}\mathbf{y} + \mathbf{g}(\mathbf{y}, \varepsilon) = \mathbf{\Lambda}\mathbf{y} + \varepsilon \mathbf{g}^{(1)}(\mathbf{y}) + \varepsilon^2 \mathbf{g}^{(2)}(\mathbf{y}) + \cdots + O(\varepsilon^{M+1}) \tag{4}$$

and use the arbitrariness of the functions $\mathbf{u}^{(m)}$ in equation (3) to make equation (4) easier to solve than equation (2).

Substituting equation (3) into equation (2) yields

$$[\mathbf{I} + D\mathbf{u}(\mathbf{y}, \varepsilon)]\dot{\mathbf{y}} = \mathscr{F}(\mathbf{y} + \mathbf{u}(\mathbf{y}, \varepsilon), \varepsilon), \tag{5}$$

‡The parameter ε is introduced here in order to facilitate the analysis of the order of magnitude in the context of asymptotic expansions.

where $D\mathbf{u} = \partial\mathbf{u}/\partial\mathbf{y}$ is the Jacobian matrix of $\mathbf{u}$ with respect to $\mathbf{y}$. Then, combining equations (4) and (5), one obtains

$$[\mathbf{I} + D\mathbf{u}(\mathbf{y}, \varepsilon)]\mathscr{G}(\mathbf{y}, \varepsilon) = \mathscr{F}(\mathbf{y} + \mathbf{u}(\mathbf{y}, \varepsilon), \varepsilon).$$

Separating in $\mathscr{F}$ and $\mathscr{G}$ the linear from the non-linear parts and rearranging the previous equation yields

$$[\mathbf{I} + D\mathbf{u}(\mathbf{y}, \varepsilon)](\mathbf{\Lambda y} + \mathbf{g}(\mathbf{y}, \varepsilon)) = \mathbf{\Lambda y} + \mathbf{\Lambda u}(\mathbf{y}, \varepsilon) + \mathbf{f}(\mathbf{y} + \mathbf{u}(\mathbf{y}, \varepsilon), \varepsilon).$$

It is possible to rewrite the previous equation as

$$D\mathbf{u}(\mathbf{y}, \varepsilon)\mathbf{\Lambda y} - \mathbf{\Lambda u}(\mathbf{y}, \varepsilon) = \mathbf{f}(\mathbf{y} + \mathbf{u}, \varepsilon) - D\mathbf{u}(\mathbf{y}, \varepsilon)\mathbf{g}(\mathbf{y}, \varepsilon) - \mathbf{g}(\mathbf{y}, \varepsilon).$$

This equation is called the *homological* equation. Returning to the expansion in terms of ε, the above equation, must be solved in the unknowns terms of near-identity-transformation terms $\mathbf{u}^{(1)}, \mathbf{u}^{(2)}, \ldots$ for each order in ε.

Note that $\mathbf{u}^{(q)}$ is a linear combination of monomial terms of the type $\mathbf{u}_{\mathbf{a}}^{(q)} = \mathbf{c}y_1^{a_1} y_2^{a_2} \ldots y_N^{a_N} = \mathbf{c}\mathbf{y}^{\mathbf{a}}$, where $\mathbf{a}^{\mathrm{T}} = (a_1, \ldots, a_N)$ with $a_1 + a_2 + \cdots + a_N = q$. Hence,

$$D\mathbf{u}_{\mathbf{a}}^{(q)}(\mathbf{y})\mathbf{\Lambda y} - \mathbf{\Lambda u}_{\mathbf{a}}^{(q)}(\mathbf{y}) = -\mathbf{E}_{\mathbf{a}}\mathbf{u}_{\mathbf{a}}^{(q)}(\mathbf{y})$$

with

$$\mathbf{E}_a = [(\lambda_i - \mathbf{a}^{\mathrm{T}}\boldsymbol{\lambda})\delta_{ik}],$$

where $\boldsymbol{\lambda}^{\mathrm{T}} = (\lambda_1, \ldots, \lambda_N)$. The resulting system is

$$\mathbf{E}_{\mathbf{a}}\mathbf{u}_{\mathbf{a}}^{(q)}(\mathbf{y}) = \hat{\mathbf{f}}_{\mathbf{a}}^{(q)}(\mathbf{y}) - \mathbf{g}_{\mathbf{a}}^{(q)}(\mathbf{y}) \tag{6}$$

with

$$\hat{\mathbf{f}}_{\mathbf{a}}^{(q)}(\mathbf{y}) = \left[\mathbf{f}^{(q)}(\mathbf{y} + \mathbf{u}) - \sum_{h=1}^{q-1} D\mathbf{u}^{(h)}(\mathbf{y})^{(q-h)}(\mathbf{y})\right]_{\mathbf{a}}$$

where, for any $\mathbf{h}$, the symbol $[\mathbf{h}]_{\mathbf{a}}$ denotes the monomial term of the type $\mathbf{c}\mathbf{y}^{\mathbf{a}}$ within $\mathbf{h}$.

Next, there exist two possibilities (for the sake of notational simplicity, the subscript in $\mathbf{a}$ is dropped in the expressions that follow). If $E_{ii} = \lambda_i - \mathbf{a}^{\mathrm{T}}\boldsymbol{\lambda}$ is large, the non-linear term $\hat{f}_i^{(q)}$ in equation (5) can be eliminated by choosing $u_i^{(q)} = \hat{f}_i^{(q)}/E_{ii}$, which obviously implies that the resonant term $g_i^{(q)}(\mathbf{y})$ is set equal to zero. On the other hand, if E_{ii} is small (see later for how small), then

$$g_i^{(q)}(\mathbf{y}, \varepsilon) = \hat{f}_i^{(q)}(\mathbf{y}, \varepsilon),$$

$u_i^{(q)} = 0$ is then chosen for sake of simplicity. In summary, the solution of equation (1) is expressed as

$$\mathbf{z} = \varepsilon(\mathbf{y} + \mathbf{u}(\mathbf{y}, \varepsilon)), \tag{7}$$

where the y_i are given by integrating equation (4) and the u_j are determined as stated above. For all the results presented, the solution is simply given as $\mathbf{z} = \varepsilon\mathbf{y}$, since the term $\mathbf{u}(\mathbf{y}, \varepsilon)$ concerns higher harmonics (multiple of the fundamental). Indeed, in the present case these are not important as validated by the comparison with the numerical results.

3. AMPLITUDE AND FREQUENCY OF LCOs

In this section, the above formulation is supplied to study the stability of a 2-d.o.f. typical section (described in terms of the pitch α and the plunge ξ) in the neighborhood of the flutter speed U_F. The formulation of this problems is obtained by considering a 2-d.o.f. airfoil, elastically constrained by a linear translational spring and non-linear torsional spring, oscillating in pitch and plunge. Using standard notations, the plunging deflection is denoted by h, positive in the downward direction, and α is the pitch angle about the elastic axis, positive with nose up. The elastic axis is located at a distance $a_h\, b$ from the mid-chord, where b is half the chord, while the mass center is located at a distance $x_\alpha\, b$ from the elastic axis. Both distances are positive when measured towards the trailing edge of the airfoil. The aeroelastic equations of motion for linear springs are found for instance in Fung [16]. Alighanbari and Price [10] extended these equations to the case in which the torsional spring is non-linear:

$$\ddot{\xi} + x_\alpha \ddot{\alpha} + 2\zeta_\xi \frac{\bar{\omega}}{U}\dot{\xi} + \left(\frac{\bar{\omega}}{U}\right)^2 \xi = -\,p(\tau), \qquad \frac{x_\alpha}{r_\alpha^2}\ddot{\xi} + \ddot{\alpha} + 2\zeta_\alpha \frac{1}{U}\dot{\alpha} + \frac{1}{U^2} M(\alpha) = r(\tau), \tag{8}$$

where the $\cdot$ denotes differentiation with respect to the non-dimensional time τ, defined as $\tau = V\,t/b$, $\xi = h/b$ is the non-dimensional plunge displacement of the elastic axis, $r_\alpha = \sqrt{J_\alpha/mb^2}$ is the radius of gyration about the elastic axis, $\bar{\mu} = \pi\rho b^2/m$ is the mass ratio and ζ_ξ, ζ_α are the viscous damping coefficients[§]; note that $M(\alpha)$ is the overall expression of the torsional spring moment, including the linear part. In equations (8), $\bar{\omega}$ is given by $\bar{\omega} = \omega_\xi/\omega_\alpha$ where ω_ξ and ω_α are the uncoupled plunging and pitching modes natural frequencies, and U is defined as $U = V/b\omega_\alpha$ where V is the dimensional speed. Moreover, $p(\tau)$ and $r(\tau)$ are the lift and pitching moment respectively. For the incompressible two-dimensional flow, Fung [16] gives the following expressions for $p(\tau)$ and $r(\tau)$ in the case of zero initial conditions:

$$p(\tau) = \frac{1}{\bar{\mu}}(\ddot{\xi} - a_h\ddot{\alpha} + \dot{\alpha}) + \frac{2}{\bar{\mu}}\int_0^\tau \phi(\tau-\sigma)\dot{w}_{3/4}(\sigma)\,\mathrm{d}\sigma,$$

$$r(\tau) = \frac{1}{\bar{\mu}r_\alpha^2}\left[a_h(\ddot{\xi}\text{-}a_h\ddot{\alpha}) - a_h\dot{\alpha} - \frac{1}{8}\ddot{\alpha}\right] + \frac{2}{\bar{\mu}r_\alpha^2}(\tfrac{1}{2} + a_h)\int_0^\tau \phi(\tau-\sigma)\dot{w}_{3/4}\,\mathrm{d}\sigma$$

with $w_{3/4}(\tau) = \dot{\xi}(\tau) + \bar{a}_h\dot{\alpha}(\tau) + \alpha(\tau)$ and $\bar{a}_h = 1/2(1 - a_h)$, where $\phi(t)$ is the Wagner function.

Utilizing the Jones [17] approximation of the Wagner function (equation (13)), the problem may be recast (see Appendix A) as a system of a six first order differential equations, as

$$\dot{\mathbf{w}} = \mathbf{A}(U)\mathbf{w} + \mathbf{r}(\mathbf{w}, U), \tag{9}$$

where $\mathbf{x} = \{\dot{\xi}, \dot{\alpha}, \dot{u}, \xi, \alpha, u\}^{\mathrm{T}}$ is the state vector, $\mathbf{A}(U)$ is the linear part of the equations of motion and $\mathbf{r}(\mathbf{w}, U)$ is the vector of non-linear terms. Setting $\mathbf{w} = \mathbf{R}\mathbf{z}$, with $\mathbf{R}$ given by the eigenvalue problem $\mathbf{A}(U_F)\mathbf{R} = \mathbf{R}\boldsymbol{\Lambda}$, the linearly diagonal format is obtained $\dot{\mathbf{z}} = \boldsymbol{\Lambda}\mathbf{z} + \mathbf{f}(\mathbf{z})$, which is the starting point for the application of the normal form technique.

In the following, as in Alighanbari and Price [10], the pitching moment is assumed to be given by a cubic function $M(\alpha) = \alpha + \beta_\alpha\,\alpha^3$.

[§]As mentioned above, the study included a deeper analysis (not reported on Figure 16), i.e. removing each individual $\hat{\lambda}$-point of the minimal set to verify its relevance to the accuracy of the solution.

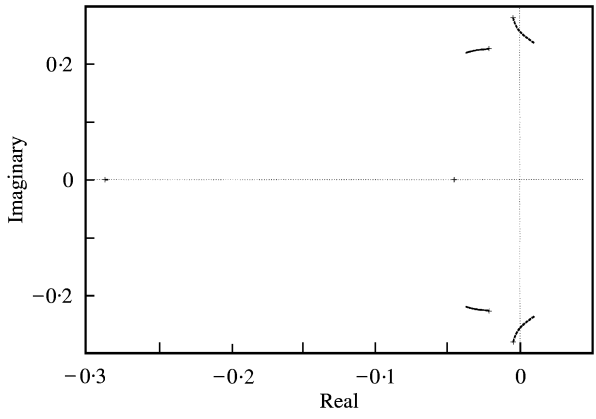

Figure 5. Root locus, eigenvalues of the linear part of equations of motion.

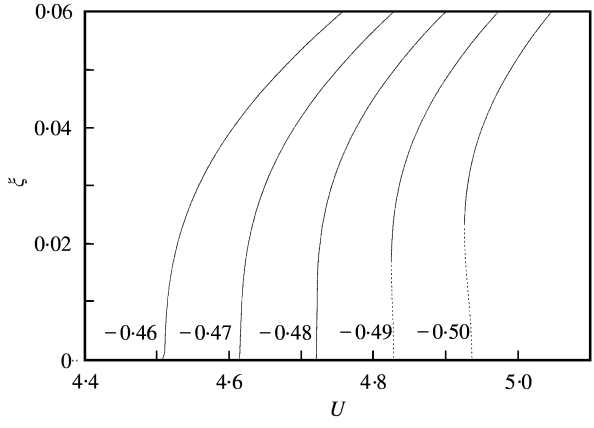

Figure 6. Plunge-mode amplitude of LCOs obtained via numerical simulation.

The results are presented here to show:

the existence of a speed range, below the linear flutter speed, such that the onset of LCOs is possible for sufficiently large initial conditions;
the dependence of the bifurcation diagram (specifically, of the existence of a turning point, i.e. a "knee" behavior) upon the position of the elastic center.

The values of the coefficients considered in this case are (see Appendix A for the definitions of the symbols) $\bar{\mu} = 100$, $x_\alpha = 0{\cdot}25$, $\bar{\omega} = 1{\cdot}2$, $r_\alpha = 0{\cdot}5$, $\zeta_\xi = 0$, $\zeta_\alpha = 0$, whereas a_h assumes different values. The flutter speed and frequency are obtained by a root-locus stability analysis; in the case of $a_h = -0{\cdot}5$, one obtains $U_F = 4{\cdot}937$ and $\omega_F = 0{\cdot}255$, as shown in the root locus depicted in Figure 5.

In Figure 6 the numerical LCO plunge-mode amplitudes, ξ, are given as functions of U, in the neighborhood of U_F, for $\beta_\alpha = -50$, and for several values of a_h (the different values of a_h correspond to different positions of the elastic center along the chord); in the dashed portion of the curves, the limit cycle is unstable. These LCO amplitudes are computed with the shooting method of reference [18] (the method is slightly modified by Dessi [15] so as to

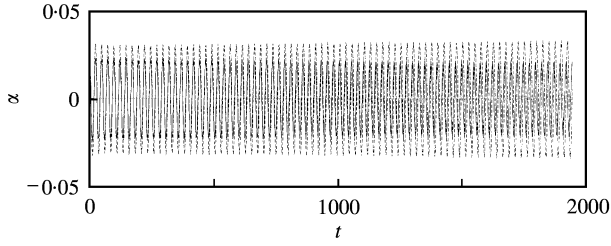

Figure 7. Time histories for plunge and pitch ($a_h = -0{\cdot}5$, $U = 4{\cdot}932$) showing initial condition UNDER the unstable LCO (——) and initial condition OVER unstable LCO (- - - - - -).

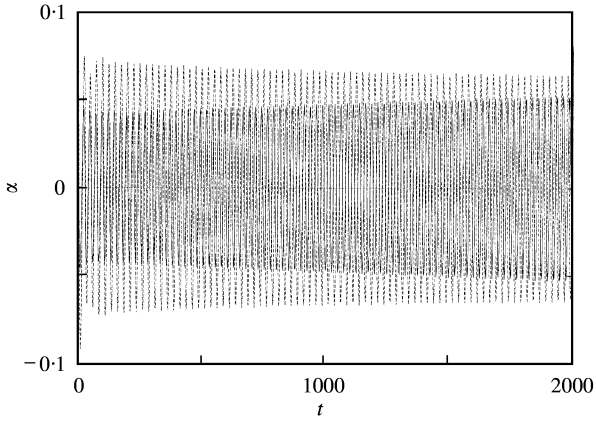

Figure 8. Time histories for pitch ($a_h = -0{\cdot}5$, $U = 4{\cdot}932$) showing initial condition UNDER the unstable LCO (——) and initial condition OVER unstable LCO (- - - - - -).

provide also the LCO period and the Floquet multipliers). It is apparent from Figure 6 how the shape of the bifurcation diagram changes with a_h; for $a_h \simeq -0{\cdot}48$, the Hopf bifurcation changes from sub-critical into super-critical, and the turning point disappears, as a_h increases. These two types of Hopf bifurcations are specific examples of the curves depicted in Figures 1 and 3, describing the growth of the LCOs amplitudes. On the basis of these results, it is possible to subdivide the state space into two different six-dimensional basins of attraction (in general, these are N-dimensional for N-dimensional dynamical systems). This fact may be more evident on examining two typical time histories for α obtained via numerical integration of equation (2) by the standard fourth-order Runge–Kutta method, for the speed value $U = 4{\cdot}932 < U_F$. These results are shown in Figures 7 and 8. The results presented in Figure 7 (Figure 8) correspond to initial conditions slightly above and below the unstable (stable) branch of the curve depicted in Figure 3 (the transient state moves toward different steady state solutions depending upon the initial conditions).

Next, one defines U_N, the non-linear instability value of U as the lowest value of U for which an instability may occur (given suitable initial conditions). Of course, in the case of the two curves on the right-hand side of Figure 6 (where a dashed portion exists), U_N corresponds to the value of U where the knee occurs (for the other curves the non-linear instability value of U coincides with U_F, the linear one). The difference between linear and non-linear stability regions in the plane of parameters U and a_h, with $a_h = (x_{EA} - x_0)/b$,

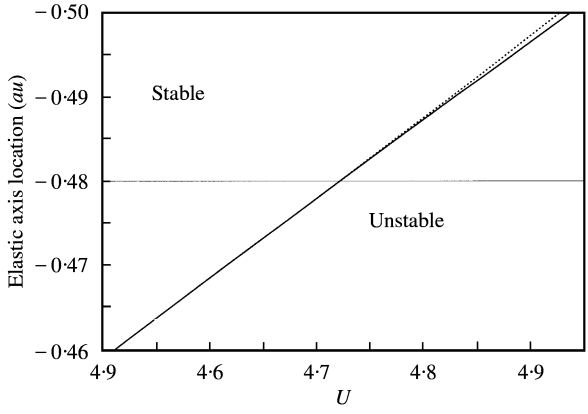

Figure 9. Linear (flutter limit, ——) and non-linear (turning point abscissa, ·····) flutter boundary.

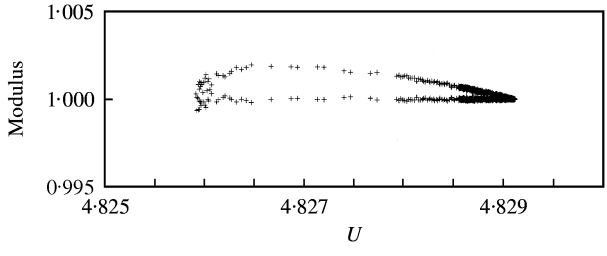

Figure 10. Floquet multipliers for stable and unstable LCO branches of the bifurcation diagram, $a_h = -0{\cdot}49$.

where x_{EA} is the abscissa of the elastic axis, x_0 that of the midchord point and b is the semichord (in particular, $a_h = -0{\cdot}5$ corresponds to the quarter-chord point, i.e. the aerodynamic center). This is shown in Figure 9. The horizontal line, $a_h = -0{\cdot}48$, corresponds to the middle curve of Figure 6 (i.e. transition from sub-critical to super-critical Hopf bifurcation). This figure shows that as the elastic center moves toward the leading edge (decreasing values of a_h), the difference between U_F and U_N increases, even though by a small amount (note: this is simply a different way, more easily understandable from a physical point of view, to present the results of Figure 6).

The stability of these LCOs may be analyzed by means of the Floquet theory (see reference [18]). The results are shown in Figure 10, which depicts (for $a_h = -0{\cdot}49$) the moduli of the critical Floquet multipliers (i.e. those with values close or equal to one; recall that if a Floquet multiplier is outside the unit circle, the corresponding LCO is unstable). In Figure 10, the moduli of the critical multipliers are shown in the neighborhood of the flutter speed: the upper branch refers to the unstable limit cycle which starts at the bifurcation point (modulus larger than one), while the lower branch refers to the stable limit cycle (into which the unstable one turns at the turning point). This figure allows an estimation (for $a_h = -0{\cdot}49$) of $U_N = 4{\cdot}8259$ and $U_F = 4{\cdot}8292$.

Next, consider the approximate limit-cycle solutions, as obtained with the normal form method outlined before, and shown in Figure 11. The solid curve corresponds to the numerical results (standard fourth order Runge–Kutta) for several values of a_h (same curves as in Figure 6). The dotted and dashed lines correspond, respectively, to third order and fifth order approximations of the limit-cycle amplitudes. It should be emphasized that these curves are obtained using only two equations, which correspond to the critical eigenvalues.

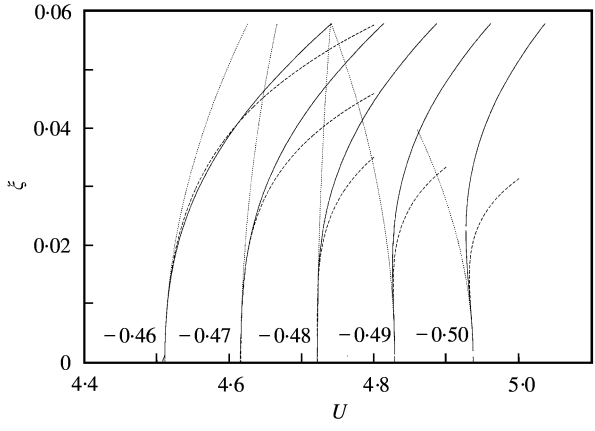

Figure 11. Fifth order (– – –) and third order (· · ·) approximation of numerical bifurcation diagrams (——), with normal-form method.

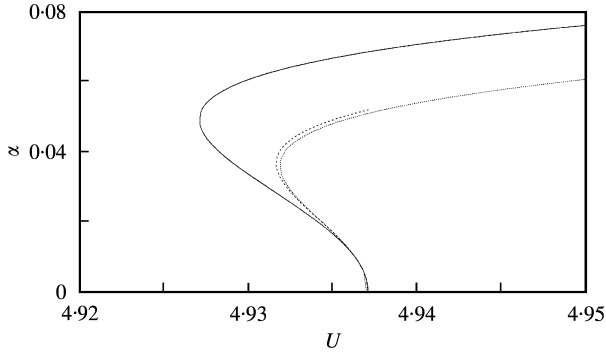

Figure 12. Bifurcation diagrams and their approximation with the normal-form and MTS methods. ——, numerical solution; ·····, fifth-order MTS approximation; - - - - - -, fifth-order NF approximation.

[This initial choice to use only two equation was motivated by past experience with third order analysis, based on the center-manifold theorem (see, e.g. references [12–19]). The main contribution of this paper is a critique to this point (see later).] One sees that the third order approximation does not capture (not even qualitatively) the 'knee-type' bifurcations. On the other hand, one sees that fifth order approximation leads to better results even for super-critical bifurcations (which occur for values of a_h greater than $-0{\cdot}48$). However, the agreement is only qualitative.

As mentioned above, the discrepancy in the curves is explained later in terms of the inadequacy of the use of two modes in the fifth order analysis. Before addressing this issue, some results obtained with an alternate singular perturbation technique are reported, the multiple time scaling. (For this method the reader is referred to references [19–22]; the results were originally presented inreference [15], to which the reader is referred for details. The motivation for presenting these results lies in the authors' desire to identify the source of the discrepancy, specifically to decide between the inadequacy of the novmel firm method and that connected with the use of the center-manifold theorem.) Figure 12 shows a satisfactory comparison between the two-mode fifth order results obtained with these two techniques (the fact that the agreement between the two perturbation sets of results is so good is a consequence of deep theoretical analogies of these techniques; see reference [15]

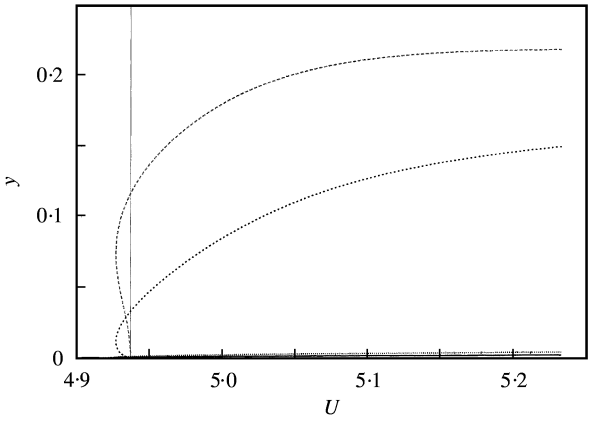

Figure 13. Generalized co-ordinates modulus in the neighborhood of U_F, results obtained by shooting method. ——, linear flutter boundary; - - - - - -, first mode (undamped, complex); - - - - - -, second mode (damped, complex) ———, third mode (damped, real) ·····, four mode (damped. real).

for a detailed discussion of this subject). However, as before, these results are in poor agreement with the numerical solution (continuous line). This indicates that both fifth order approximations are not adequate in the neighborhood of U_F. As stated above (and shown in the next paragraph), this is due to the fact that, in obtaining the approximate solution, one has used a two-mode analysis, which appears inadequate for a fifth order analysis (while it is for the third order one).

Specifically, in obtaining the above results, the normal form perturbation technique has been applied under the mistaken assumption that the modes to be used are those identified by the center-manifold theorem (i.e. the linearly undamped modes). As shown in Figure 13, in the case of a fifth order approximation (required for identifying the turning point), this assumption is clearly violated even for small values of $U - U_F$, since the first pair of damped modes (unknowns y_3 and y_4), negligible in a third order analysis, becomes relevant in a fifth order analysis (the other two modes, i.e. unknowns y_5 and y_6, are negligible for the fifth order as well). This is true even below the linear flutter speed—indeed the term "postcritical" is not to be referred to the values of $U - U_F$—but rather to the values of ε, which is related to the limit cycle amplitude (note that it is possible to have finite values of even for $U - U_F = 0$, see Figure 13).

This implies that in using the perturbation analysis the contribution of other complex state variables should be included. This issue was investigated by defining, for the sake of conciseness,

$$\hat{\lambda} = \hat{\lambda}(i, j_1, \ldots, j_m) = \lambda_i - \mathbf{a}^{\mathrm{T}}\boldsymbol{\lambda} \tag{10}$$

where $\hat{\lambda}\,(i, j_1, \ldots, j_m)$ is here designated as the $\hat{\lambda}$-point. The $\hat{\lambda}$-points are plotted in Figure 14 for every combination of $i, j_1, \ldots, j_m$ (each one corresponding to a different non-linear term), for $U = U_F$. One established, by trial and error, that the $\hat{\lambda}$-points inside the curve depicted in Figure 15 (a blow-up of the region around the origin in Figure 14) could be considered as "near-resonant" (i.e. "small divisors" in Poincaré's terminology); in other words, this is the minimal set of equations that yields a good agreement between the solution of the normal-form equations and that of the original equations. Specifically, if one increased the number of $\hat{\lambda}$-points no difference was observed; on the other hand, if any of the $\hat{\lambda}$-points in the minimal set was removed, substantial deterioration was obtained—indeed, for some

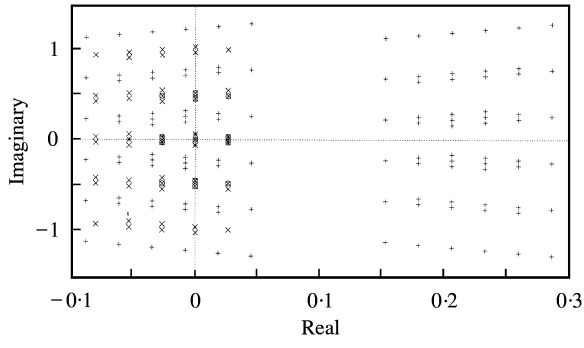

Figure 14. Numerical LCO frequencies versus speed: comparison with imaginary part of the eigenvalues ($a_h = -0{\cdot}5$). Key for $\hat{\lambda}$-points: linear terms ○; cubic terms ×; quintic terms +.

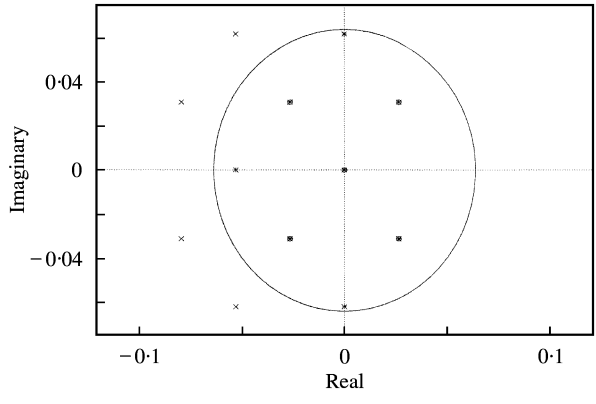

Figure 15. Numerical LCO frequencies versus speed: comparison with normal form approximation ($a_h = -0.5$). circle Key for $\hat{\lambda}$-points; linear terms ○; cubic terms, ×; quintic terms, +.

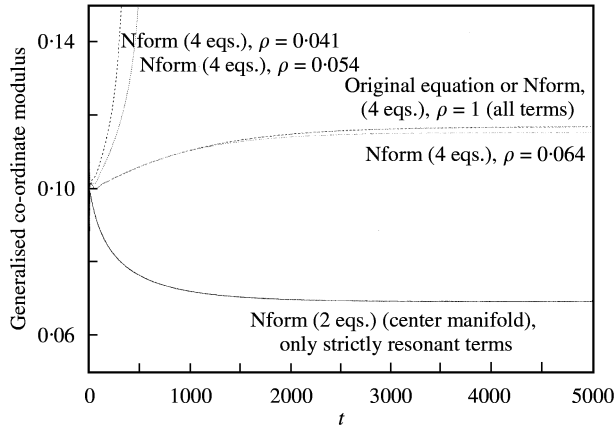

Figure 16. Time histories of the generalized co-ordinate modulus for different normal-form approximations.

choices, instabilities were observed. It is worth noting that the curve in Figure 15 is a circle: this fact is used in Figure 16, where the time history $|y_1|$ (this implies the amplitude of the critical mode, as obtained by the time marching integration of the normal form equation), is plotted for different values of ρ (i.e. adding more and more non-linear terms until

TABLE 1

List of the $\hat{\lambda}$-points belonging to the minimal set with the following positions $\lambda_1 = \mathrm{i}\omega_1$, $\lambda_3 = \beta + \mathrm{i}\omega_3$ and $\Delta\omega = \omega_1 - \omega_3$

Equation	$I_{i,q}$	Index combinations (all permutations)	λ-points associated to each term of the minimal set	Formal value
$i = 1$	$I_{1,1} =$	{1,	$\lambda_1 - \lambda_1$	0
		3}	$\lambda_1 - \lambda_3$	$-\beta + \mathrm{i}\Delta\omega$
	$I_{1,3} =$	{{112},	$\lambda_1 - \lambda_1 - (\lambda_1 + \lambda_2)$	0
		{114},	$\lambda_1 - \lambda_1 - (\lambda_1 + \lambda_4)$	$-\beta - \mathrm{i}\Delta\omega$
		{123},	$\lambda_1 - \lambda_1 - (\lambda_2 + \lambda_3)$	$-\beta + \mathrm{i}\Delta\omega$
		{134}}	$\lambda_1 - \lambda_1 - (\lambda_3 + \lambda_4)$	-2β
	$I_{1,5} =$	{{11122},	$\lambda_1 - \lambda_1 - 2(\lambda_1 + \lambda_2)$	0
		{11223},	$\lambda_1 - \lambda_1 - (\lambda_1 + \lambda_2) - (\lambda_2 + \lambda_3)$	$-\beta + \mathrm{i}\Delta\omega$
		{11124},	$\lambda_1 - \lambda_1 - (\lambda_1 + \lambda_2) - (\lambda_1 + \lambda_4)$	$-\beta - \mathrm{i}\Delta\omega$
		{11234}}	$\lambda_1 - \lambda_1 - (\lambda_1 + \lambda_2) - (\lambda_3 + \lambda_4)$	-2β
$i = 3$	$I_{3,1} =$	{3,	$\lambda_3 - \lambda_3$	0
		1}	$\lambda_3 - \lambda_1$	$-\beta - \mathrm{i}\Delta\omega$
	$I_{3,3} =$	{{123},	$\lambda_3 - \lambda_3 - (\lambda_1 + \lambda_2)$	0
		{112},	$\lambda_3 - \lambda_1 - (\lambda_1 + \lambda_2)$	$\beta - \mathrm{i}\Delta\omega$
		{233},	$\lambda_3 - \lambda_3 - (\lambda_2 + \lambda_3)$	$-\beta + \mathrm{i}\Delta\omega$
		{134},	$\lambda_3 - \lambda_1 - (\lambda_3 + \lambda_4)$	$-\beta - \mathrm{i}\Delta\omega$
		{334},	$\lambda_3 - \lambda_3 - (\lambda_3 + \lambda_4)$	-2β
		{114}}	$\lambda_3 - \lambda_1 - (\lambda_1 + \lambda_4)$	$-2\mathrm{i}\Delta\omega$
	$I_{3,5} =$	{{11223},	$\lambda_3 - \lambda_3 - (\lambda_1 + \lambda_2) - (\lambda_1 + \lambda_2)$	0
		{11122},	$\lambda_3 - \lambda_1 - 2(\lambda_1 + \lambda_2)$	$\beta - \mathrm{i}\Delta\omega$
		{11234},	$\lambda_3 - \lambda_3 - (\lambda_1 + \lambda_2) - (\lambda_1 + \lambda_4)$	$-\beta - i\Delta\omega$
		{12233},	$\lambda_3 - \lambda_3 - (\lambda_1 + \lambda_2) - (\lambda_2 + \lambda_3)$	$-\beta + i\Delta\omega$
		{12334},	$\lambda_3 - \lambda_3 - (\lambda_1 + \lambda_2) - (\lambda_3 + \lambda_4)$	2β
		{11124}}	$\lambda_3 - \lambda_4 - (\lambda_1 + \lambda_2) - 2\lambda_1$	$-2\mathrm{i}\Delta\omega$

a satisfactory solution is obtained[¶]). Good agreement with the full-system solution is achieved for $\rho = 0{\cdot}064$. This value of ρ is such that no contribution is given by the equations for y_5 and y_6. Thus the equations used are

$$\begin{aligned} \dot{y}_1 &= \sum_{p \in I_{1,1}} a_{1p} y_p + \sum_{pqr \in I_{1,3}} c_{1pqr} y_p y_q y_r + \sum_{pqrst \in I_{1,5}} e_{1pqrst} y_p y_q y_r y_s y_t, \\ \dot{y}_3 &= \sum_{p \in I_{3,1}} a_{3p} y_p + \sum_{pqr \in I_{3,3}} c_{3pqr} y_p y_q y_r + \sum_{pqrst \in I_{3,5}} e_{3pqrst} y_p y_q y_r y_s y_t, \end{aligned} \tag{11}$$

where $y_2 = \bar{y}_1$, and $y_4 = \bar{y}_3$. The index combinations $I_{i,q}$ are defined in Table 1, which gives a detailed list of the selected $\hat{\lambda}$-points of the minimal set.

A summary of the results is given in Figure 17, where the absolute value of the LCO (complex) amplitudes of y_1 and y_3 (critical and linearly damped modes), obtained by the normal form method (four modes), are given for some values of U; the lines refer to numerical integration results (where the shooting method was employed).

Additional information about the non-linear behavior of the system regards the LCO frequencies. Note that such frequencies depend strongly upon the velocity. For the linear

[¶]The damping coefficients ζ_α, ζ_ξ are set to zero throughout the paper; they are considered here for sake of completeness.

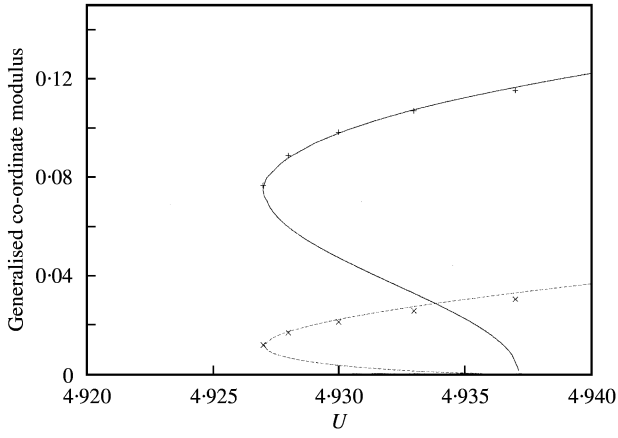

Figure 17. Fifth order approximation of numerical bifurcation diagrams with the modified normal-form method for critical and damped modes. Key for modes: ——, critical/numerical; – – – – damped/numerical; +, critical/NForm; ×, damped/NForm.

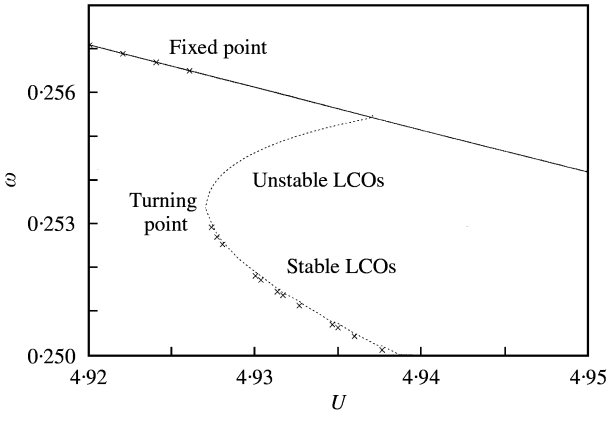

Figure 18. Numerical LCO frequencies versus speed: comparison with imaginary part of the eigenvalues (linear problem, $a_h = -0.5$). Key: ——, linear problem; – – – – –, shooting method; ×, Fourier transform.

analysis with velocities less than the flutter speed $U_F = 4{\cdot}937$, the signal is damped; in this case, the frequency of oscillation is simply given by the imaginary part of the corresponding eigenvalues. As shown in Figure 18 (solid line), the dependency is linear (this is true even for $U > U_F$, where the signal grows exponentially). For the non-linear analysis, the LCO frequency depends upon the velocity in a manner completely different from that of the linear case. Figure 18 depicts also the LCO frequencies (for both stable and unstable limit cycles) as functions of the flight speed, in the neighborhood of the linear flutter speed (dashed line and crosses). Specifically, these results were obtained using two methods: (i) the Fourier Transform of the numerical simulation obtained *a la* Runge–Kutta (crosses; for $U < U_K$, where U_k is the turning-point abscissa, the numerical solution is that corresponding to the linear analysis), and (ii) the shooting method (also from the numerical-simulation solution; dashed line). As one can see, the LCO frequency, in this last case, is not correlated to the imaginary part of the critical eigenvalues (continuous line); instead, it is distributed along a parabolic-like curve (as a function of $U - U_F$). This fact is confirmed by the multiple time

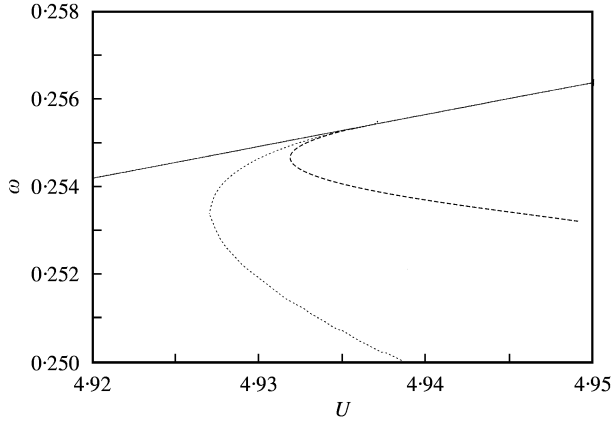

Figure 19. Numerical LCO frequencies versus speed: comparison with normal form approximation ($a_h = -0{\cdot}5$). ——, normal form (third order); · · · ·, shooting method and fifth order (four nodes) ------, normal form (fifth order, two modes).

scale method which indicates $\omega = \omega_0 + \varepsilon^2\omega_2 + \varepsilon^4\omega_4 + \cdots$, with $\varepsilon = \varepsilon(U - U_F)$, where ω_0 is the imaginary part of the critical eigenvalues, and ω_2, ω_4 are coefficients obtained with third order and fifth order analysis respectively [23].

Finally, consider the results obtained using the normal form technique. These are shown in Figure 19. The dashed line represents the correct frequencies of the LCO solution as obtained by applying the shooting method (same as in Figure 18); the continuous, straight line is the third order, normal form approximation of the LCO frequencies, whereas the dashed line is the fifth order approximation based on the center-manifold equation. The crosses give the LCO frequency corresponding to the four-mode normal-form analysis. As before, the two mode fifth order normal-form analysis captures the behavior of the solution but only qualitatively, whereas in order to obtain quantitatively accurate results (crosses) the normal form based on the minimal set criterion (four-mode analysis) must be used.

4. CONCLUDING REMARKS

In this paper the phenomenon of limit-cycle stability reversal in the neighborhood of a Hopf bifurcation has been addressed. This phenomenon corresponds to a turning point (knee) in the curve of the LCO amplitude as a function of the stability parameter, μ. The test case used is that of a typical section with a non-linear spring, undergoing flutter. However, the results are presented to believed to have a general validity and are summarized here. Two methods are used in this analysis. The first is based upon the numerical integration (standard fourth order Runge–Kutta method) of all the equations of motion. The second is based on the numerical integration of a reduced number of the normal-form equations. In both cases, the shooting method was employed (in an extended form that allows one to obtain not only LCO amplitudes, but also LCO frequencies and LCO Floquet multipliers).

In order to identify the number of equations to be used for the normal form analysis, we starts with those identified from the center-manifold theorem. This gives results which agreed with those of the original equations only qualitatively. This was confirmed by the multiple-scale results for the same equations. One then noticed, from the numerical results based on the original equations, that the contributions from the modes disregarded in the center-manifold analysis were not all negligible.

The analysis was then repeated by looking at the small divisors for the complete set of the equations. The (original) conclusion is that good agreement between the analysis based upon the completed and the reduced set of equations is obtained including certain terms. The terms to be included correspond to a certain combination of the eigenvalues of the linear system, here designated as λ-points: these are in close relationship with the concept of small divisors in the KAM theory for Hamiltonian systems (in this case the λ-points have zero real part and the imaginary part coincides with the small divisors). Note that the same criterion (small divisors or near resonance) is used in both: (i) determining the minimal set of equations, and (ii) determining the minimal set of non-linear terms.

Additional work appears desirable in order to provide a deeper understanding of the λ-point issues (and its relationship with the KAM small-divisors theory). Also the study of more general types of equations is warranted, along with applications of other types of physical problems.

REFERENCES

1. J. Guckenheimer and P. Holmes 1983 *Nonlinear Oscillations, Dynamical Systems, and Bifurcations of Vector Fields*. New York: Springer-Verlag.
2. B. H. K. Lee and A. Tron 1989 *Journal of Aircraft* **26**, 781–786. Effects of structural nonlinearities on flutter characteristics of the CF-18 aircraft.
3. M. Lacabanne 1997 *Proceedings of the CEAS International Forum of Aeroelasticity and Structural Dynamics, Rome*, Vol. 3, 239–246. An experimental analysis of the aeroelastic behaviour with a freeplay in a control surface.
4. H. Matsushita, K. Saitoh and P. Granasy 1998 *AIAA*-98-1728, 267–273. Wind tunnel investigation of transonic limit cycle fLutter.
5. P. C. Chen, D. Sarhaddi and D. D. Liu 1998 *AIAA*-98-1727, 258–266. Limit-cycle-oscillations studies of a fighter with external stores
6. H. Matsushita, E. Mosekilde, L. E. Christiansen, T. Lehn-Schiò Ler and P. Gránásy, 2001 *Proceedings of the International Forum on Aeroelasticity and Structural Dynamics, IFASD* 2001, *Madrid*, Vol. **2**, 287–294, Examination of the two-degrees-of-freedom nonlinear math model for transonic flutter.
7. D. S. Woolston, H. L. Runyan and R. E. Andrews 1957 *Journal of Aeronautical Sciences* **24**, 57–63. An investigation of certain types of structural nonlinearities on wing and control surface flutter.
8. S. F. Shen 1958 *Journal of Aeronautical Sciences* **26**, 25–32. An approximate analysis of nonlinear flutter problems.
9. Z. C. Yang and L. C. Zhao 1988 *Journal of Sound and Vibrations* **123**, 1–13. Analysis of limit cycle flutter of an airfoil in incompressible flow.
10. H. Alighanbari and S. J. Price 1996 *Nonlinear Dynamics* **10**, 381–400. The post-hopf-bifurcation response of an airfoil in incompressible two-dimensional flow.
11. B. H. L. Lee, L. Jiang and Y. S. Wong 1998 *AIAA*-98-1725, 237–257. Flutter of an airfoil with a cubic nonlinear restoring force.
12. L. Morino 1969 *American Institute of Aeronautics and Astronautics Journal* **7**, 405–411. A perturbation method for treating nonlinear panel flutter problem.
13. L. Smith and L. Morino 1976 *American Institute of Aeronautics and Astronautics Journal* **14**, 333–341. Stability analysis of nonlinear differential autonomous system with applications to flutter.
14. A. Erdelyi 1956 *Asymptotic Expansions* New York: Dover Publications.
15. D. Dessi 1999 *Ph.D. Thesis in Aerospace Engineering, University of Rome La Sapienza*. Analisi teorica and numerica del fenomeno del flutter nonlineare.
16. Y. C. Fung 1969 *An Introduction to the Theory of Aeroelasticity*. New York: Dover Publications.
17. R. T. Jones 1940 *NACA Report* 681. The unsteady lift of a wing of finite aspect ratio.
18. A. H. Nayfeh and B. Balachandran 1995 *Applied Nonlinear Dynamics*. New York: John Wiley Sons.
19. A. H. Nayfeh 1965 *Journal of Mathematics and Physics* **44**, 368–374. A perturbation method for treating nonlinear oscillation problems.

20. G. SANDRI *Nuovo Cimento* **B36**, 67–93. A new method of expansion in mathematical physics.
21. J. D. COLE and J. KEVORKIAN 1963 *Nonlinear Differential Equations and Nonlinear Mechanics*, 113–120, New York: Academic Press. Uniformly valid asymptotic approximations for certain nonlinear differential equations.
22. D. DESSI, L. MORINO and F. MASTRODDI 1997 *Proceedings of the CEAS International Forum on Aeroelasticity and Structural Dynamics Rome*, Vol. 3, 355–362. A fifth-order no-reconstruction multiple-scale solution for Hopf bifurcations.
23. D. DESSI, L. MORINO and F. MASTRODDI 1999 *Proceedings of the International Conference of Engineering Aero-Hydroelasticity Prague*, 135–140. Linear vs. nonlinear stability behavior of an aeroelastic system in the neighborhood of a Hopf bifurcation.
24. V. I. ARNOLD 1978 *Metodi Geometrici della Teoria delle Equazioni Differenziali Ordinarie, Moscow*, (translated in Italian: Editori Riuniti—Ed. Mir, Mosca).
25. S. WIGGINS 1990 *Introduction to Applied Nonlinear Dynamical Systems and Chaos Texts in Applied Mathmatics*. New York: Springer-Verlag.
26. S. CHOW and J. K. HALE 1982 *Methods of Bifurcation Theory*. New York: Springer-Verlag.
27. C. VENKATESAN and P. P. FRIEDMANN 1986 *American Institute of Aeronautics and Astronautics Journal* **24**, 1889–1897. New Approach to finite-state modeling of unsteady aerodynamics.

APPENDIX A

Because of the existence of the integral term in the expression of aerodynamic forces, classical methods for investigating stability properties of dynamical systems do not work: for example, the system stability near equilibrium points cannot be analyzed readily since most of the available methods for nonlinear dynamical systems are developed for ordinary differential equations. In order to eliminate the integral term, a new variable is defined as

$$u(\tau) = \int_0^\tau \phi(\tau - \sigma)\dot{w}_{3/4}(\sigma)\,\mathrm{d}\sigma. \tag{A.1}$$

The aim of successive algebraic manipulations in the Laplace domain (all the equations are Laplace-transformed) is to rewrite this relationship as a differential equation in the unknown function $u(\tau)$[‖]. In the following, Laplace-transformed terms will be denoted by $\tilde{}$, while the Laplace variable is denoted with the letter 's'.

The Laplace transform of equation (A.1) is $\tilde{u}(s) = \tilde{\phi}(s)\, s\, \tilde{w}_{3/4}(s)$, whereas the Jones [17] approximation of the Wagner function in the Laplace domain is

$$\tilde{\phi}(s) = 1/s - \hat{a}/(s + \hat{b}) - \hat{c}/(s + \hat{d}), \tag{A.2}$$

with $\hat{a} = 0{\cdot}165$, $\hat{b} = 0{\cdot}0455$, $\hat{c} = 0{\cdot}335$ and $\hat{d} = 0{\cdot}3$[††] After some algebraic manipulation, equation (A.1) in the Laplace domain (with zero for all the space-state variables) becomes

$$(s^2 + e_{10}s + e_{11})\,\tilde{u}(s) = (e_{13}s^2 + e_{12}s + e_{11})[s\tilde{\xi}(s) + s\bar{a}_h\tilde{\alpha}(s) + \tilde{\alpha}(s)], \tag{A.3}$$

with

$$e_{10} = \hat{b} + \hat{d}, \qquad e_{11} = \hat{b}\hat{d}, \qquad e_{12} = \hat{b} + \hat{d} - \hat{b}\hat{c} - \hat{a}\hat{d}, \qquad e_{13} = 1 - \hat{a} - \hat{c}.$$

At this point, the equations of motion (8) in the Laplace domain are given by

$$e_1\, s^2\, \tilde{\xi} + e_2 s^2\, \tilde{\alpha} + e_3\, s\, \tilde{\xi} + e_4\, s\, \tilde{\alpha} + e_5\, \tilde{\xi} = -\,\tilde{u}, \quad e_6\, s^2\, \tilde{\xi} + e_7\, s^2\, \tilde{\alpha} + e_8\, s\, \tilde{\alpha} + e_9\, \tilde{M} = e_{14}\, \tilde{u}$$

[‖]Note that the same procedure can be developed in the time domain, as well, but the procedure is cumbersome in the frequency domain.

[††]More accurate approximations are provided by Venkatesan and Friedmann [27]. One employs the approximation by Jones [17] used by Alighanbari *et al.* [10], make comparisons.

with

$$e_1 = 1/2(1+\bar{\mu}), \quad e_2 = 1/2(-a_h + \bar{\mu}x_\alpha) \quad e_3 = \bar{\mu}\zeta_\xi \bar{\omega}/U, \quad e_4 = 1/2, \quad e_5 = 1/2\bar{\mu}(\bar{\omega}/U)^2,$$
$$e_6 = -a_h + \bar{\mu}x_\alpha, \quad e_7 = 1/8 + a_h^2 + \bar{\mu}r_\alpha^2, \quad e_8 = \bar{a}_h + 2\bar{\mu}\zeta_\alpha r_\alpha^2/U,$$
$$e_9 = \bar{\mu}(r_\alpha/U)^2, \quad e_{14} = 1 + 2a_h.$$

Explicating the s^2-terms, one obtains derivatives

$$\begin{aligned} s^2\tilde{\xi} &= a_{41}\tilde{\xi} + a_{43}\tilde{u} + a_{44}s\tilde{\xi} + a_{45}s\tilde{\alpha} + f_4\tilde{M}, \\ s^2\tilde{\alpha} &= a_{51}\tilde{\xi} + a_{53}\tilde{u} + a_{54}s\tilde{\xi} + a_{55}s\tilde{\alpha} + f_5\tilde{M}, \end{aligned} \tag{A.4}$$

where

$$a_{41} = -e_5e_7/\bar{e}, \quad a_{43} = -(e_7 + e_2e_{14})/\bar{e}, \quad a_{44} = -e_3e_7/\bar{e},$$
$$a_{45} = -(e_4e_7 - e_2e_8)/\bar{e}, \quad a_{51} = e_5e_6/\bar{e}, \quad a_{53} = (e_6 + e_1e_{14})/\bar{e},$$
$$a_{54} = e_3e_6/\bar{e}, \quad a_{55} = -(e_1e_8 - e_4e_6)/\bar{e}, \quad f_4 = e_2e_9/\bar{e},$$
$$f_5 = -e_1e_9/\bar{e}, \quad \bar{e} = e_1e_7 - e_6e_2.$$

It is possible to note in equation (A.3) the existence of s^3-terms. Thus, combining equations (A.4) and (A.3), with the aim of eliminating the second and third derivatives of α and ξ, it is possible to obtain the final equation for u containing s^2-terms only:

$$s^2\tilde{u} = a_{61}\tilde{\xi} + a_{62}\tilde{\alpha} + a_{63}u + a_{64}s\tilde{\xi} + a_{65}s\tilde{\alpha} + a_{66}s\tilde{u} + f_6\tilde{M} + f_7s\tilde{M}'\tilde{\alpha}, \tag{A.5}$$

where

$$a_{61} = a_{41}[e_{12} + e_{13}(a_{44} + a_{54})] + a_{51}[e_{12} + e_{13}(1 + a_{45} + a_{55})], \quad a_{62} = e_{11},$$
$$a_{63} = -e_{11} + a_{43}[e_{12} + e_{13}(a_{44} + a_{54})] + a_{53}[e_{12} + e_{13}(1 + a_{45} + a_{55})]$$
$$a_{64} = e_{11} + e_{13}(a_{41} + a_{51}) + a_{44}[e_{12} + e_{13}(a_{44} + a_{54})] + a_{54}[e_{12} + e_{13}$$
$$(1 + a_{45} + a_{55})],$$
$$a_{65} = e_{11} + e_{12} + a_{45}[e_{12} + e_{13}(a_{44} + a_{54})] + a_{55}[e_{12} + e_{13}(1 + a_{45} + a_{55})],$$
$$a_{66} = e_{13}(a_{43} + a_{53}) - e_{10}, \quad f_6 = f_4[e_{12} + e_{13}(a_{44} + a_{54})] + f_5[e_{12} + e_{13}$$
$$(1 + a_{45} + a_{55})], \quad f_7 = e_{13}(f_4 + f_5).$$

The inverse Laplace transform may be applied to equations (A.4) and (A.5), yielding a system of three second order differential equations, which may be easily recast in the first order form, equation (9).